Silica Nanoparticle-based Photoresin for THz High-Resolution 3D Microfabrication by Two-Photon Polymerization

Magaway, Emil; Farahi, Yeganeh; Hanham, S. M.; Zhang, Jason; Guaidia-Moreno, Adriana; Navarro-Cia, Miguel

DOI:
10.1109/TTHZ.2023.3275282

Citation for published version (Harvard):
Magaway, E, Farahi, Y, Hanham, SM, Zhang, J, Guaidia-Moreno, A & Navarro-Cia, M 2023, 'Silica Nanoparticle-based Photoresin for THz High-Resolution 3D Microfabrication by Two-Photon Polymerization', *IEEE Transactions on Terahertz Science and Technology*, vol. 13, no. 4, pp. 415-418.
https://doi.org/10.1109/TTHZ.2023.3275282

THz Letters

Silica Nanoparticle-based Photoresin for THz High-Resolution 3D Microfabrication by Two-Photon Polymerization

Emil John Y. Magaway, Yeganeh Farahi, Stephen M. Hanham, *Member, IEEE*, Zhenyu J. Zhang, Adriana Guaidía-Moreno and Miguel Navarro-Cía, *Senior Member, IEEE* .

***Abstract*—Two-photon polymerization is a promising fabrication technique for complex three-dimensional (3D) structures operating at TeraHertz (THz) given its sub-μm resolution with hundreds of mm^3 print volume capability. However, standard photoresins exhibit unsuitably high THz absorption and have poor mechanical, chemical, and thermal stability. To address the latter three issues, a new photoresin (commercially known as GP-Silica) based on silica nanoparticles dispersed in a photocurable binder matrix has been recently developed. To assess its suitability for THz devices, we report the THz dielectric properties of GP-Silica and compare them with standard 3D printable materials. We find that GP-Silica outperforms the other photoresins by almost 5 times in terms of absorption, which finally unlocks additive manufacturing for THz applications.**

***Index Terms*—3D printing, two-photon polymerization, THz dielectric properties.**

I. Introduction

ADDITIVE manufacturing (AM) refers to the process by which the formation of a structure is achieved through successive layers of one or more materials [1]. Various techniques of AM have been developed in recent years [2] with only a few succeeding in fabricating sub-THz devices such as stereolithography [3], [4] and micro laser sintering [5], because of the stringent dimensional accuracy and surface finish requirements above 100 GHz [6]. To meet the even more stringent requirements of THz devices, the only solution seems to be two-photon polymerization (TPP), whereby three-dimensional (3D) micro- and nano-structures are printed in a photosensitive resin using a femtosecond laser beam [7]. The appeal of TPP for THz devices is its unmatched sub-μm resolution, print volume capability and minimal surface roughness. However, available photoresins used with TPP are too lossy in the THz range rendering their use for realising dielectric structures impractical. As the interest in THz radiation grows [8], so too does the demand for THz devices capable of bringing concepts into practice. One of the key challenges in forming these devices is finding low-loss materials which can guide THz radiation with minimal absorption.

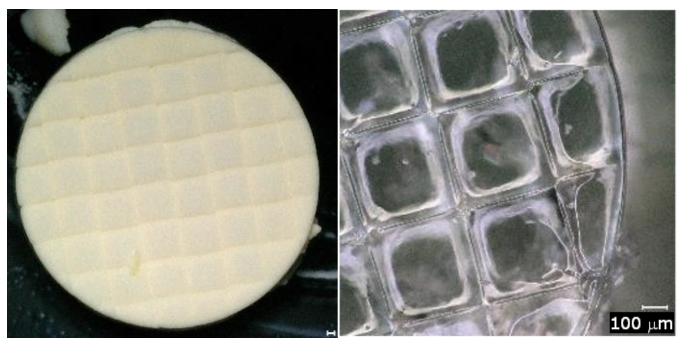

Fig. 1. 3 mm diameter GP-Silica sample: pre-sintering (left) and post-sintering (right). Scale bar: 100 μm.

This letter presents the dielectric properties of a photoresin based on silica nanoparticles dispersed in a photocurable binder matrix called GP-Silica. Figure 1 shows a TPP printed sample which has been subsequently sintered to form a bulk material for characterisation. Dielectric properties of other resins and inorganic materials are also provided for the purposes of comparison.

II. Materials and Method

A. THz System

The dielectric properties of five photoresins were characterized using a commercial THz-TDS system (Toptica TeraFlash Pro Dual) set in transmission mode with a four parabolic mirror configuration [9]. Through a 0.1 mm step two-dimensional raster scan of a 0.2 mm pinhole [10], the beam waist in the focal plane was estimated to be 0.9, 0.7, 0.5 and 0.4 mm at 1, 1.5, 2 and 2.5 THz, respectively.

A scan duration of 100 ps, with 0.05 ps time step, was used for all data collection. The spectrum in the time domain was

This work was supported in part by the UKRI Engineering and Physical Sciences Research Council (EPSRC) [Grant Nos. EP/S018395/1 and EP/V001655/1] and the Royal Society [Grant No. IEC/NSFC/191104].
(*Corresponding author: Miguel Navarro-Cía*).

E. J. Y. Magaway and Y. Ferahi are with the School of Physics and Astronomy, University of Birmingham, Birmingham B15 2TT, United Kingdom.

S. M. Hanham is with the Department of Electronic, Electrical and System Engineering, University of Birmingham, Birmingham B15 2TT, United Kingdom.

Zhenyu J. Zhang is with the School of Chemical Engineering, University of Birmingham, Birmingham B15 2TT, United Kingdom.

Adriana Guaidía-Moreno is with Nanoscribe GmbH & Co. KG, 76344 Eggenstein-Leopoldshafen, Germany

M. Navarro-Cía is with the School of Physics and Astronomy, and the Department of Electronic, Electrical and System Engineering, University of Birmingham, Birmingham B15 2TT, United Kingdom. (e-mail: M.Navarro-Cia@bham.ac.uk)

Manuscript received XX YY, 2023; revised XX YY, 2023.

obtained by averaging 100 trace pulses whilst no averaging was carried out in the frequency domain as it was seen not to greatly improve the signal-to-noise ratio (SNR) [11].

B. Sample Preparation

The materials tested were GP-Silica, IP-Q and IP-S from Nanoscribe, and Enduro RGB450 and Veroblue from Stratasys; sample thicknesses can be found in Table I. GP-Silica sample fabrication followed two steps. Initially the desired geometry was printed from GP-Silica using a Photonic Professional GT2 (PPGT2) with the 3D Large Feature Solution Set, 10x objective and Silicon substrate, with slicing and hatching distances (the distance between laser scanned layers, and the distance between centre lines of two successive laser scans in each layer, respectively) of 5 and 1 μm, respectively. Any unpolymerized material was washed away by immersing the sample in methanol for 10 min, followed by isopropanol for 1 min and final air dry, resulting in the sample shown on the left hand side of Fig. 1; the polymerized binder matrix was removed at 600°C. The sample was then sintered at 1,300°C using a DEKEMA Austromat 674S; this stage observed a reduction in volume of the printed structure (see Fig. 1) of $\sim 45\%$ as the silica nanoparticles fused to become silica glass.

IP-Q and IP-S samples were prepared by pipetting liquid resin onto a glass slide and placing under a UV lamp until solidified. Enduro RGB450 and Veroblue were 3D printed in-house using stereolithography (Stratasys Objet30 Prime).

TABLE I
SAMPLE THICKNESSES

Sample	GP-Silica	IP-Q	IP-S	Enduro	Veroblue
Thickness (μm)	550 - 570	1230	1140	2020	2010

C. GP-Silica Characterization

To fabricate a 3000 μm diameter sample of GP-Silica, 3D blocks 300 x 300 μm in length and width, were stitched together, as illustrated in Fig. 1. To confirm whether the boundaries between individual blocks caused any scattering that may have affected the retrieval of dielectric properties, the sample was probed through varying size pinholes (200 – 2500 μm). By using a range of pinhole sizes, the area illuminated by the THz pulse was varied from less than an individual block to almost the entirety of the sample.

Results from these experiments are provided in Fig. 2 and confirm the negligible impact of scattering from block boundaries. Note that the data for the 200 μm pinhole begins at a higher frequency to observe the high-pass filter effect of such a small pinhole; for perspective, the frequency cut-off of a 200 μm diameter waveguide is approximately 0.9 THz. The other materials tested were considered to be homogeneous and have smooth surfaces and hence were not probed with varying size pinholes.

D. Data Retrieval

The samples' dielectric properties as described by the refractive index (n) and absorption coefficient (α), or real (ϵ_r) and imaginary (ϵ_{im}) parts of the complex relative permittivity (ϵ^*), were extracted through Fourier transformation of the time domain data [12]. The relationship between these parameters is displayed in Eqs. 1 - 3.

$$\epsilon^* = \epsilon_r - i\epsilon_{im} = (n^2 - \kappa^2) - i(2n\kappa) \tag{1}$$

$$tan\delta = \frac{\epsilon_{im}}{\epsilon_r} = \frac{2n\kappa}{n^2 - \kappa^2} \tag{2}$$

$$\alpha(\omega) = 2\frac{\omega\kappa(\omega)}{c} \tag{3}$$

where κ is the extinction coefficient and c is the speed of light.

By solving the transfer function of samples in the frequency domain, $H(\omega)$ given in Eq. 4, taking into account Fabry-Perot effects as shown in Eq. 5, the desired data was obtained.

$$\begin{aligned} H(\omega) &= \frac{E_s(\omega)}{E_{ref}(\omega)} \\ &= \frac{4n(\omega)}{[n(\omega)+1]^2} \cdot e^{-\kappa(\omega)\frac{\omega L}{c}} \cdot e^{-i[n(\omega)]\frac{\omega L}{c}} \cdot FP(L,\omega) \end{aligned} \tag{4}$$

$$\begin{aligned} FP(L,\omega) &= \sum_{j=0}^{\infty}[(\frac{n(\omega)-1}{n(\omega)+1})^2 \cdot e^{-i2n(\omega)\frac{\omega L}{c}}]^j \\ &= \frac{1}{1-(\frac{n(\omega)-1}{n(\omega)+1})^2 \cdot e^{-i2n(\omega)\frac{\omega L}{c}}} \end{aligned} \tag{5}$$

Here, L is the thickness of the sample and FP(L, ω) is the Fabry-Perot term [13].

Data was analysed within the frequency range where SNR was adequate, which varied between samples but still allowed for comparisons to be made. n, α, ϵ_r and tanδ were extracted iteratively using the Teralyzer software.

III. RESULTS AND DISCUSSION

Figure 2 presents the refractive index and real part of permittivity of the five materials tested, namely GP-Silica, IP-Q, IP-S, Enduro RGB450, and Veroblue, as well as the ones obtained from the pinhole study with errors. All materials show low levels of dispersion over the tested frequency range, with GP-Silica exhibiting slightly higher values in both parameters: n ranges between 1.94 to 1.96 and ϵ_r ranges from 3.78 to 3.83. Even using the lowest estimate for refractive index and real part of permittivity for GP-Silica, it is still 1.2 - 1.4 times larger than the next best material, Veroblue. This feature could be useful for device miniaturisation purposes.

The lower absorption coefficient and loss tangent of GP-silica in contrast with the other materials (see Fig. 2) is consistent with its potential as a low-loss material for THz. At 1 THz, GP-Silica has an absorption coefficient between 1.6 cm^{-1} and 4.0 cm^{-1}, while IP-Q, IP-S, Enduro and Veroblue have values of 19.31 cm^{-1}, 23.46 cm^{-1}, 24.42 cm^{-1} and 22.93 cm^{-1}, respectively. As can be seen from these results, even the largest estimate for the α of GP-Silica is considerably smaller than those of the other materials. This outcome remained consistent at higher frequencies; looking at 1.5 THz where absorption is slightly greater, both Enduro and Veroblue experience an increase in absorption coefficients at 42.51 cm^{-1} and 40.03 cm^{-1}, respectively, while that of GP-Silica also enlarges but still remains on the lower end reaching values between 7.45 cm^{-1} to 9.36 cm^{-1}. The GP-Silica sample, at 3 THz, obtains a maximum estimated α value of 26.1 cm^{-1}. Between 1 to 1.5 THz the loss tangent of GP-Silica increases from 0.0037 - 0.010 to 0.013 - 0.015. Regardless of this increase, as with the absorption coefficient data, it still shows the lowest values of the materials tested.

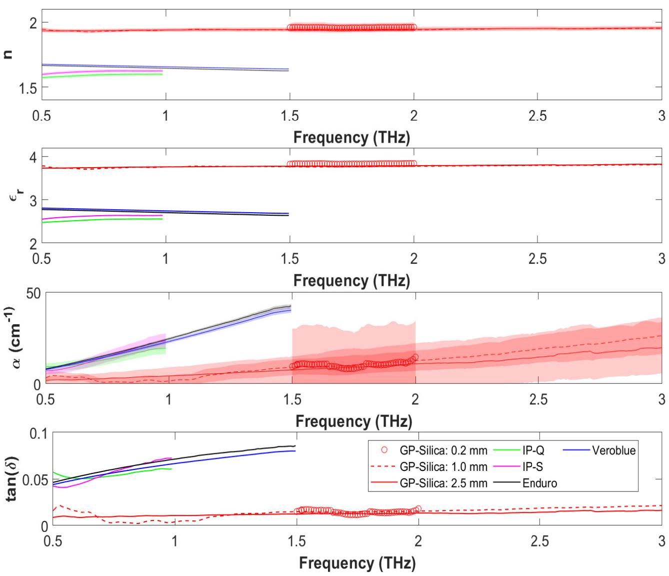

Fig. 2. In descending order, refractive index, relative permittivity, absorption coefficient and loss tangent with shaded regions representing error associated with the standard deviation - which is negligible in some cases. The results presented for each sample are averages calculated through 3 - 5 independent measurements.

As for the scattering effects of the boundaries between GP-Silica blocks, for both parameters, the data set for different pinhole sizes all fall within the error margin of each other, suggesting that there is no significant statistical difference between them. Thus, the assumption of negligible scattering effects due to boundaries holds true.

Well known THz low loss materials such as fused silica and high resistivity silicon have n values of 1.96 and 3.41 and α of 2.5 cm^{-1} and < 1 cm^{-1} at 1 THz, respectively [11], [14]. Whilst GP-Silica presents dielectric properties comparable to those of fused silica due to its high silica content, its loss properties are an order of magnitude higher than those of high resistivity silicon. However, the mechanical properties of pure fused silica and high resistivity silicon do not allow them to be machined into the complex geometries required for many THz devices. With the dielectric properties GP-Silica presents, it could find uses in optics and wave-guiding structures in applications where low to moderate losses can be accepted (e.g., THz on-chip interconnects).

The minimum feature size achievable with the TPP 3D printing technique is highly dependent on the objective and resin employed. In the case of GP-Silica with 10x objective, the minimum feature size is $\sim$20 μm with minimum surface roughness $R_a \leq 20$ nm. The maximum build volume is limited by the PPGT2's stage movement of 100 mm $\times$ 100 mm $\times$ 8 mm.

IV. Conclusion

The dielectric properties of several AM materials, including GP-Silica, were determined using a THz-TDS system. Values of refractive index, absorption coefficient, real part of permittivity and loss tangent were obtained in the range between 0.5 and 3 THz. It was observed that GP-Silica had an absorption coefficient (and, equally, loss tangent) almost 5 times smaller than any of the other representative AM materials investigated at 1 THz and the difference further increased at higher frequencies. Above 1.5 THz, GP-Silica outperformed any bulk AM material reported in the literature in terms of absorption by at least one order of magnitude. The combination of low to moderate absorption and additive manufacturability via high resolution TPP makes GP-Silica an attractive solution for complex THz devices.

References

[1] T. D. Ngo, A. Kashani, G. Imbalzano, K. T. Nguyen, and D. Hui, "Additive manufacturing (3D printing): A review of materials, methods, applications and challenges," *Composites Part B: Engineering*, vol. 143, pp. 172–196, 2018.

[2] C. Tomassoni, O. A. Peverini, G. Venanzoni, G. Addamo, F. Paonessa, and G. Virone, "3D Printing of Microwave and Millimeter-Wave Filters: Additive Manufacturing Technologies Applied in the Development of High-Performance Filters with Novel Topologies," *IEEE Microwave Magazine*, vol. 21, no. 6, pp. 24–45, 2020.

[3] U. Beaskoetxea, S. Maci, M. Navarro-Cía, and M. Beruete, "3-D-Printed 96 GHz bull's-eye antenna with off-axis beaming," *IEEE Transactions on Antennas and Propagation*, vol. 65, no. 1, pp. 17–25, 2017.

[4] T. Skaik, C. Viegas, J. Powell, B. Alderman, P. G. Huggard, H. Wang, C. Leonard, and Y. Wang, "125 GHz Frequency Doubler Using a Waveguide Cavity Produced by Stereolithography," *IEEE Transactions on Terahertz Science and Technology*, vol. 12, no. 2, pp. 217–220, 2022.

[5] T. Skaik, Y. Wang, M. Salek, P. Hunyor, H. Wang, P. G. Huggard, T. Starke, M. Attallah, and R. Martinez, "A 3-D Printed 300 GHz Waveguide Cavity Filter by Micro Laser Sintering," *IEEE Transactions on Terahertz Science and Technology*, vol. 12, no. 3, pp. 274–281, 2022.

[6] M. Almeshehe, N. Murad, M. Rahim, O. Ayop, N. Samsuri, M. Abd. Aziz, and M. Osman, "Surface roughness impact on the performance of the 3D metal printed waveguide coupler at millimeterwave band," *Engineering Science and Technology, an International Journal*, vol. 35, no. 13, p. 101129, 2022.

[7] X. Zhou, Y. Hou, and J. Lin, "A review on the processing accuracy of two-photon polymerization," *AIP Advances*, vol. 5, no. 3, p. 030701, 2015.

[8] G. Carpintero, L. E. García Muñoz, H. L. Hartnagel, S. Preu, and A. V. Räisänen, Eds., *Semiconductor Terahertz Technology*. Wiley, 2015.

[9] Toptica Photonics Inc., "TERAFLASH pro Time-Domain Terahertz Spectroscopy Platform Manual," Tech. Rep., 2021. [Online]. Available: http://www.toptica.com

[10] S. Freer, A. Gorodetsky, and M. Navarro-Cia, "Beam Profiling of a Commercial Lens-Assisted Terahertz Time Domain Spectrometer," *IEEE Transactions on Terahertz Science and Technology*, vol. 11, no. 1, pp. 90–100, 2021.

[11] M. Naftaly, *Terahertz Metrology*. Artech House, 2015.

[12] M. Ma, Y. Wang, M. Navarro-Cía, F. Liu, F. Zhang, Z. Liu, Y. Li, S. M. Hanham, and Z. Hao, "The dielectric properties of some ceramic substrate materials at terahertz frequencies," *Journal of the European Ceramic Society*, vol. 39, no. 14, pp. 4424–4428, 2019.

[13] W. Withayachumnankul and M. Naftaly, "Fundamentals of measurement in terahertz time-domain spectroscopy," *Journal of Infrared, Millimeter, and Terahertz Waves*, vol. 35, no. 8, pp. 610–637, 2014.

[14] J. Dai, J. Zhang, W. Zhang, and D. Grischkowsky, "Terahertz time-domain spectroscopy characterization of the far-infrared absorption and index of refraction of high-resistivity, float-zone silicon," *Journal of the Optical Society of America B*, vol. 21, no. 7, p. 1379, 2004.